Multi-arm Robotic Swimming with Octopus-inspired Compliant Web

Michael Sfakiotakis, Asimina Kazakidi, Avgousta Chatzidaki, Theodoros Evdaimon and Dimitris P. Tsakiris

***Abstract*— This paper presents an 8-arm compliant robot, able to propel itself underwater by movements of its arms, either alone or interconnected via a passively-compliant web. The robot is inspired by the morphology and outstanding locomotor capabilities of the octopus, and is fabricated primarily from compliant materials. This robotic swimmer is first investigated computationally via dynamical models capturing the arm and web compliance, and indicating the effect of various kinematic parameters of the system on its motion. The performance of the robotic prototype is, then, tested experimentally, to demonstrate this novel mode of underwater propulsion by combining various patterns of sculling movements of the arms and web. Speeds of 0.5 body lengths per second and propulsive forces of up to 10.5 N were achieved, with a cost of transport as low as 0.62.**

***Index Terms*— Biologically-Inspired Robots, Soft Robots, Underwater Robots, Octopus.**

I. INTRODUCTION

The development of sophisticated underwater robotic vehicles, able to approach the efficiency and adaptability of biological organisms in an aquatic environment, could greatly enhance robotic applications like the inspection of underwater structures, search and rescue operations or the exploration of marine ecosystems. Towards this goal, we address the design of multi-functional manipulator arms, that could be used underwater both for manipulation and for propulsion, inspired by the outstanding capabilities of the octopus [1]–[4]. In addition to object manipulation and crawling, the octopus employs its arms to swim via a distinctive locomotion pattern, called *arm-swimming*, which differs from the better-known jetting employing the siphon [5]–[7]. Arm-swimming can lead to bursts of substantial forward thrust, which the octopus exploits during hunting or escape.

In [8]–[10], we presented an approximation of this biological motion, which we termed *sculling*. This involves a two-stroke motion of the arms, one in which all arms open slowly outwards with respect to the body axis (recovery stroke) and one in which the arms close rapidly inwards (power stroke), while rotating around their bases. Robotic prototypes, that could propel themselves underwater with the use of rigid arms, were also presented.

This work was supported in part by the EC/ERDF and the GSRT of the Ministry of Education via the BIOSYS-KRIPIS project [MIS-448301 (2013SE01380036)], by the ESF-GSRT HYDRO-ROB Project [PE7(281)], and by the Greek Operational Program Education and Lifelong Learning of the NSRF - Research Funding Program: THALES via the BioLegRob Project [Mis: 379424].

M. Sfakiotakis, A. Kazakidi, A. Chatzidaki, T. Evdaimon and D.P. Tsakiris are with the Institute of Computer Science, Foundation for Research and Technology – Hellas (FORTH), N. Plastira 100, Vassilika Vouton, GR-70013, Heraklion, Greece. M. Sfakiotakis is also with the Dept. of Electrical Engineering, Technological Educational Institute of Crete, Heraklion, Greece. {sfakios, kazakidi, avgousta, evdemon, tsakiris}@ics.forth.gr.

However, this work did not consider an important component of the arm-swimming behavior, namely the role of the interbranchial membrane, also called the *web*, a flexible muscular membrane that extends between the arms of octopodiform cephalopods (octopuses and vampire squids), and whose size and morphology may differ among different species. In the present paper, we develop computational models and robotic prototypes to study the effect of arm compliance and of the web on robotic arm-swimming. Our results indicate that significant velocity, thrust and efficiency can be achieved, especially with the addition of the web, by this bio-inspired robot morphology, whose compliance guarantees its smooth and safe interaction with the environment. Moreover, performance with respect to its rigid analogues needs not be sacrificed, provided appropriate design and control choices are made, using our computational and experimental studies as guidelines. In related works, we have developed detailed computational models of the elastodynamics [11], [12] and the hydrodynamics [13]–[15] of the octopus arm, explicitly taking into account its morphology and continuous nature. These novel models may contribute to the design, development and control of soft robotic systems [16].

To the best of the authors' knowledge, no other octopus-inspired robotics works address arm-swimming with compliant arms and web. However, some analogous ideas appear in underwater robots like the *Robojelly* and *Cyro* robots of Virginia Tech [17], [18], and the Festo *AquaJelly* device [19]. These interesting robots are inspired by the jellyfish, which has distinctly different swimming characteristics from the octopus, and appear to achieve primarily straight-line vertical displacements. An important difference of our prototype is that it has several controlled degrees of freedom, and is capable of both straight-line and turning movements, via a variety of swimming gaits including arms and web, which might be exploited towards generating reactive behaviors.

Section II of the paper describes computational models that account for the compliant arms and web, and are employed in Section III in a series of simulations investigating the generation of possible swimming gaits and the parameters affecting propulsion. Section IV presents the design of an eight-arm robotic swimmer with a web, and its fabrication mainly from compliant materials. Robotic swimming is demonstrated and studied parametrically using this swimmer in Section V.

II. COMPUTATIONAL MODELS

The present study extends our previous models of an eight-rigid-arm swimming robot [9], [10], to include arm compliance, as well as the effect of a web between the arms.

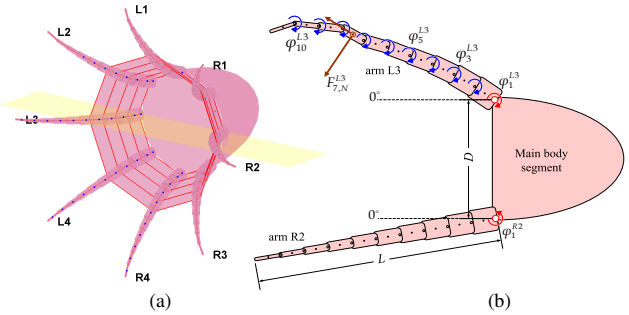

Fig. 1: (a) Model of the 8-arm swimmer, indicating the segmented compliant arms and web. (b) Planar view of a pair of diametrically opposite arms. The rotary joints connecting the base arm segments to the main body (shown in red) are actuated, while the other joints are passive, and feature spring-and-damper elements.

A. Mechanical model

The SIMUUN computational environment [20], which is based on the SimMechanics toolbox of Simulink, is used to set up these models, whose configuration and mechanical parameters are specified to reflect those of the robotic prototypes described in Section IV. The arms are attached to the rear of a main body (shaped as a half ellipsoid with diameter D and half-length D), arranged axi-symmetrically at $45°$ intervals, and oriented so that each pair of diametrically-placed arms moves in the same plane (Fig. 1). Each arm is modeled as a kinematic chain of $n = 10$ cylindrical rigid segments, interlinked by 1-dof planar rotary joints. Unlike our previous studies [8]–[10], the segment interlinking joints (i.e., for $i = 2..10$ in Fig. 1b) are here considered to be unactuated, and are equipped with rotary linear spring-and-damper elements, the parameters of which can be adjusted to describe the flexibility of different materials used for the arms. In accordance with the experimental prototype (c.f. Section IV), the joint for the base ($i = 1$) segment, which connects the arm to the main body in the model is assumed to be actively driven by an appropriate actuator that enables prescribing a specific angular trajectory for it.

To model web-equipped variants of the 8-arm system, the approach adopted here involves flexible strips interconnecting the ith segment (where $i = 1..4$) of each arm with the corresponding ith segment of its neighboring arm (see Fig. 1a). Each of these strips is constrained so that its center of mass remains at all times on the line that connects the centers of mass of the corresponding segments of the two arms to which the strip is attached.

B. Fluid drag model

The modeled system is assumed to move within quiescent fluid, so that hydrodynamic forces acting on a single arm segment result only from its motion, as detailed in [8]–[10]. The above approach is employed for modeling the fluid interactions of the main body, as well as that of the web. Estimates for the corresponding drag force coefficients were obtained using standard hydrodynamics formulas for flow over a hemisphere and a thin plate, respectively [21]. The fluid force model in the simulation also takes into account the changing surface of the trapezoidal-shaped web strips, which varies according to the angular position of the arm segments during the propulsive motions described below.

C. Gait generation

The basic motion profile adopted for the movement of individual arms is based on a two-stroke *sculling* pattern, of different velocity ratio β between a relatively slow opening part (recovery stroke) and a considerably faster closing part (power stroke) of the arms. This motion pattern can be considered as a first approximation of the octopus arm-swimming motion.

The sculling motion involves specifying the angular trajectory $\varphi_1(t)$ of the actuated joint connecting each arm to the body, according to the two-stroke acceleration profile presented in [9] (cf. Fig. 3). The main parameters of this motion are the angular amplitude A, its angular offset ψ and the maximum angular velocity during the recovery stroke ω. The duration of the power and the recovery stroke are $T_p = 2.5A/(\beta\omega)$ and $T_r = \beta T_p$, respectively, while the overall period of the sculling motion is $T_s = T_p + T_r = (\beta + 1)T_p$.

For flexible arms, simulated through selecting appropriate values for the parameters of the spring-and-damper elements in the unactuated joints ($i = 2..N$), the angular trajectories of the latter (and, hence, the overall arm shape) evolve in response to the sculling motion of the base segment, as a function of the hydrodynamic loading, the damping joint torques and the inertial characteristics of the segments.

The above profile, employed as a basic motion template for the arms, gives rise to a variety of different sculling *gaits*, for both forward [9] and turning [10] motions of the system. Some of the most effective ones, for locomotion along a straight line, are:

G1 gait: all eight arms move in synchrony, each performing the above sculling motion profile.

G2 gait: synchronized sculling movement of pairs of diagonally opposite arms (i.e., $\{L1, R4\}$, $\{L2, R3\}$, $\{L3, R2\}$, and $\{L4, R1\}$, cf. Fig. 1a) with a phase difference of $T_s/4$ between adjacent pairs of arms.

G4 gait: synchronized sculling movement of two sets of four arms, one set containing four non-adjacent arms and the other set the remaining non-adjacent arms (i.e., $\{L1, R2, R4, L3\}$ and $\{R1, R3, L4, L2\}$), with a phase difference of $T_s/2$ between the two sets of arms.

A variety of turning gaits have also been developed for our system, by introducing appropriate asymmetries in the above sculling motion patterns, as detailed in [10].

III. COMPUTATIONAL STUDIES

The computational framework detailed in the previous Section was employed in simulation studies, to assess the effect on propulsive efficacy of the web and the arm flexibility, with respect to the various kinematic parameters of the sculling-based gaits for straight-line swimming. Regarding the latter, we focus here on the effect of the amplitude A and the offset ψ of the sculling motion, retaining as constants the other two parameters with $\omega = 50\,°/\mathrm{s}$ and $\beta = 5$.

A. Arm-only swimming

The simulations performed to investigate swimming by the use of the arms alone considered two different configurations, with respect to the arm compliance, in accordance with the experimental studies described in Section V. The first configuration (referred to as *stiff*) involved relatively large stiffness for the passive arm joints, which resulted in limited bending motions of the arm (mainly near its tip) during swimming. The spring coefficient of the joints was specified in the range of $0.63 - 0.015\,\mathrm{Nm/rad}$ (gradually decreasing from the arm base towards its tip), while the viscous damping coefficient was set at $0.12{\cdot}10^{-3}\,\mathrm{Nm\cdot s/rad}$ for all joints, to simulate the polyurethane arms used in the robotic prototype (cf. Section V). In the second configuration (referred to as *flexible*), the spring-and-damper parameters were specified to simulate the behavior of the silicone-made set of arms employed in the robotic prototype, which exhibit more extensive bending motions. The range for the joints' spring coefficients employed in this case was from $62.8{\cdot}10^{-3}$ to $0.3\cdot10^{-3}\,\mathrm{Nm/rad}$ (base to tip), with a uniform viscous damping coefficient of $0.12\cdot10^{-3}\,\mathrm{Nm\cdot s/rad}$.

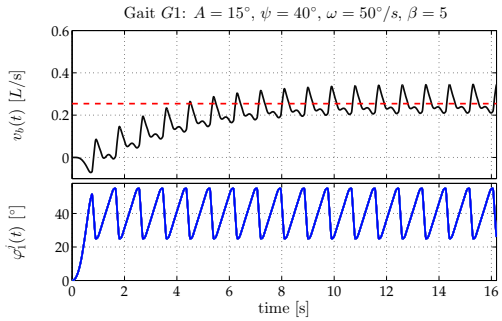

(a) Gait $G1$ with flexible arms

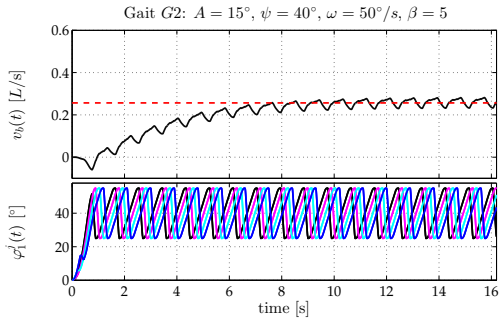

(b) Gait $G2$ with flexible arms

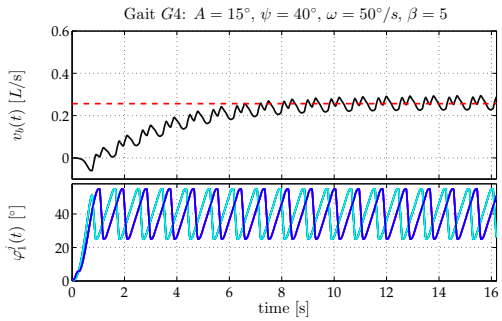

(c) Gait $G4$ with flexible arms

Fig. 2: Simulation results: Instantaneous axial velocity v_b (normalized by the arm length L) of the flexible-arms system, shown against the arms' sculling trajectories, for gaits $G1$, $G2$, and $G4$. The dashed red line denotes the average steady-state velocity V.

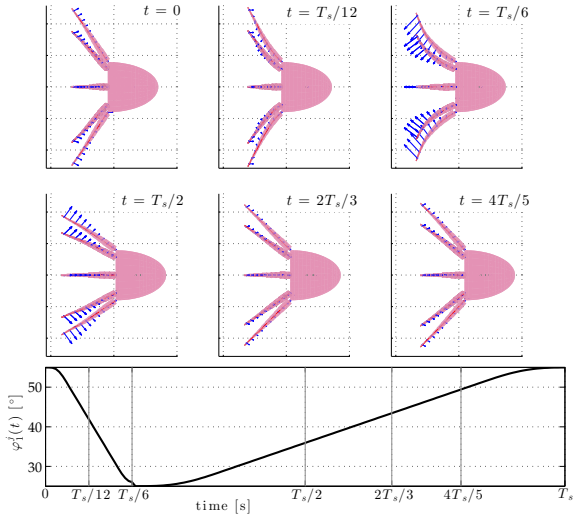

Fig. 3: Simulation results: Visualization of the system with the flexible arms, swimming with gait $G1$, for $A = 15°$, $\psi = 40°$. The blue arrows denote velocities. The snapshots concern different (non-regularly spaced) time instances of one sculling period, whose correspondence with the angular trajectory of the base segment is provided in the lower plot.

Indicative simulation results, demonstrating forward propulsion by gaits $G1$, $G2$ and $G4$, using the flexible arms, are shown in Fig. 2, for $A = 15°$ and $\psi = 40°$. Although the average steady-state velocity V is approximately the same for the three gaits, the different patterns for the coordination of the arms' sculling motion have a significant impact on the profile of the instantaneous velocity $v_b(t)$. In gait $G1$, the latter exhibits characteristics peaks that coincide with the power stroke of the arms' synchronized motions. On the other hand, the phasing of the arms' power strokes in $G2$ results in thrust generation being evenly distributed over the duration of T_s. The variations of $v_b(t)$, which occur with a period equal to $T_s/4$, are considerably reduced, resulting in a quite smooth overall forward motion of the system. Correspondingly, the phasing of gait $G4$ yields a velocity profile with characteristics that fall in-between those of the other two gaits. The snapshots from the simulation, shown in Fig. 3, provide an illustration of the flexible arms' bending motion over one sculling period, for gait $G1$.

In addition, Fig. 4 shows the response obtained for the system with the stiff arms, swimming using gait $G1$. The average velocity is slightly higher in comparison to the one obtained with the flexible arms (cf. Fig. 2a). Also, the characteristic peak during the power stroke, associated with the activation pattern of the arms in $G1$, is more pronounced.

The average velocities V attained by the system at steady-state, for different sculling offsets and amplitudes, with the two types of arms are summarized in Fig. 5. Similar to our findings for propulsion with rigid arms [9], the results for the stiff arms (solid lines in Fig. 5) indicate that A appears

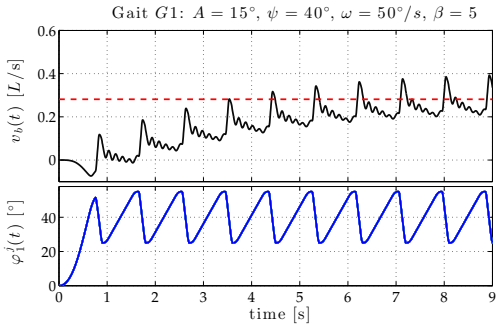

Fig. 4: Simulation results: Instantaneous axial velocity v_b (normalized by the arm length L) of the system with the stiff arms, shown against the arms' sculling trajectories, for gait $G1$. The dashed red line denotes the average steady-state velocity V.

to have limited influence on V, while the optimal value for ψ is near $40°$. However, it is noted that the variance of V with respect to ψ is, in this case, reduced in comparison to what was observed for the rigid arms. This is also the case for the results of the flexible arms (dashed lines in Fig. 5).

B. Arm swimming with the web

Simulations to assess the effect of the web on the propulsion characteristics of the system considered the $G1$ forward sculling gait, while employing the flexible arms. In order to capture the increase in the arms' stiffness from the presence of the web, the spring coefficients for the first four segment interlinking joints ($i = 2..5$) were increased by a factor of 5, compared to their specified values for when the flexible arms are used without the web. The velocity profile and corresponding simulation snapshots, obtained with this setup for $A = 15°$, $\psi = 15°$, are provided in Figs. 6-7, respectively. Compared to the results shown in Figs. 2a and 4, the web can be seen to have a significant effect on the velocity profile, which exhibits considerable variance over the sculling period.

In addition, the average steady-state velocity of the system, for different values of A and ψ, is shown in Fig. 8. Compared to the data from the simulations of swimming only with the arms (cf. Fig. 5), these results indicate that significantly higher velocities are attainable with the use of the web. The results also suggest a strong dependence of V on the sculling offset, as the velocity drops off at a significant rate from its maximum value (attained for small values of ψ), for

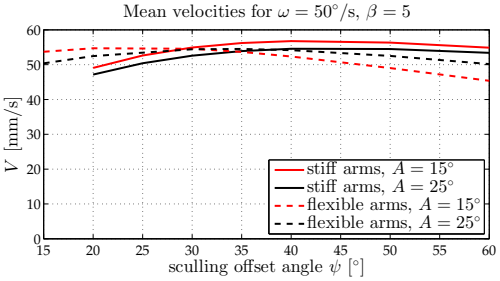

Fig. 5: Simulation results: Variation of the average attained forward velocity V for the two types of arms, for gait $G1$, as a function of the sculling offset ψ, for different sculling amplitude A.

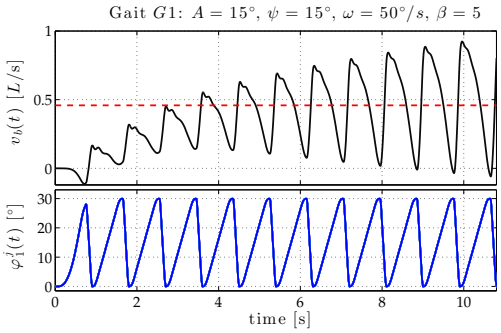

Fig. 6: Simulation results: Instantaneous axial velocity v_b (normalized by the arm length L) of the system with the web and flexible arms, shown against the arms' sculling trajectories, for gait $G1$. The dashed red line denotes the average steady-state velocity V.

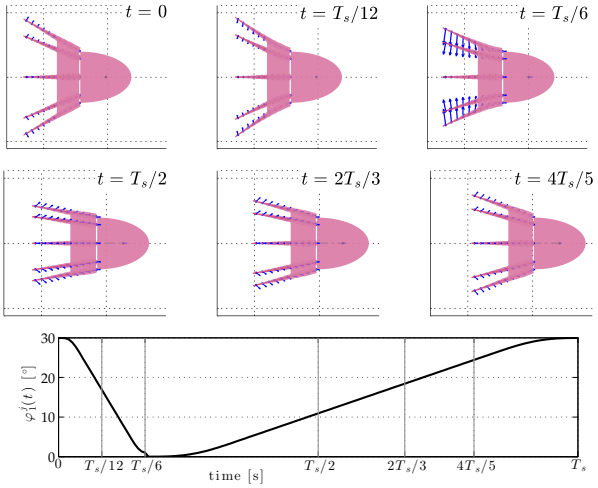

Fig. 7: Simulation results: Visualization of the system with the web and flexible arms, swimming with gait $G1$, for $A = 15°$, $\psi = 15°$, shown over one sculling period.

increasing ψ. This represents a marked difference from the characteristics exhibited for swimming only with the arms in Fig. 5, where the effect of the offset angle is rather limited.

IV. EXPERIMENTAL SETUP

A new robotic prototype (Figs. 9) was designed and fabricated mainly from compliant materials, as opposed to the rigid robots of [8]–[10]. The prototype is comprised of eight compliant arms, mounted to the rear of a platform, that encapsulates the battery and electronics (Fig. 9a), and hosts an octopus-like mantle at the front. All parts are

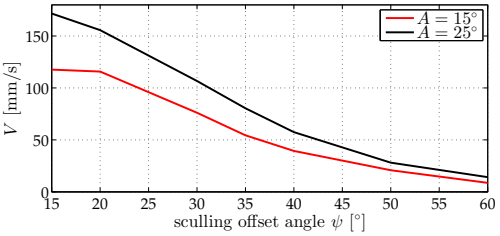

Fig. 8: Simulation results: Variation of the average forward velocity V attained with the use of the web, for gait $G1$, as a function of the sculling offset ψ, for a sculling amplitude $A = 15°$.

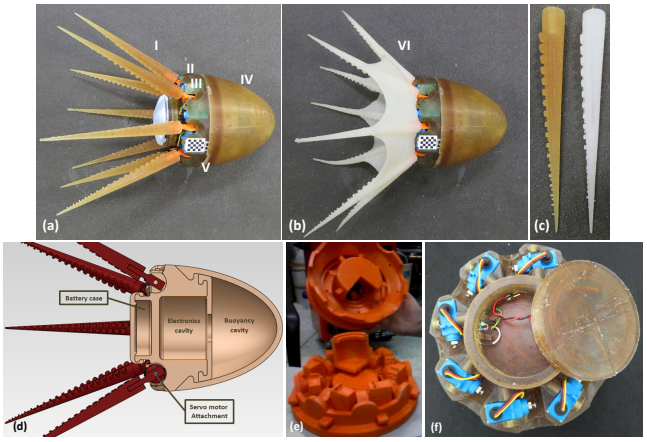

Fig. 9: The compliant 8-arm robotic prototype with (a) the PU arms and (b) the silicone arms with the passively-compliant web. (c) Individual PU and silicone arms. Latin numerals are: (I) polyurethane arms, (II) compliant platform, (III) servomotors, (IV) mantle, (V) checkerboard marker, (VI) web. (d) Schematic of the robotic prototype indicating the internal cavities. (e) Custom-designed mold for the platform. (f) The cast PU platform with the servomotors in place and the battery space.

made of Polyurethane (PU, PMC-746 urethane rubber), after being cast in molds, which were designed in SolidWorks® and printed in a 3D printer (Elite, Dimension, USA) using ABSplus material (Fig. 9b,c). A mixture of liquid urethane was poured in the molds, at room temperature, avoiding air entrapment, and was left overnight to cure. An additional set of arms was fabricated from soft silicone rubber (Dragon Skin Q), and a third set, also from silicone, which included a silicone octopus-like web in-between the arms (Fig. 9b). Each arm has a conical shape with base radius of $10\,\mathrm{mm}$, tip radius of $1\,\mathrm{mm}$, and length of $200\,\mathrm{mm}$, and includes a staggered array of 38 cylindrical sucker-like protrusions along its length, that cover about one third of the arm's surface area [13]. The arms are driven by dedicated waterproof micro-servomotors (HS-5086WP, Hitech, USA) that allow a $110°$ span of rotation. They are arranged symmetrically at the rear side of the platform (inserted in custom-made compartments, Fig. 9d), such that diametrically opposite arms move in the same plane and with the protrusions-side facing inwards. The platform has a circular shape of diameter $16\,\mathrm{cm}$, while the octopus-like mantle is a half-ellipsoid with major and minor axes of $16\,\mathrm{cm}$ and $8\,\mathrm{cm}$, respectively. The mantle encloses an empty cavity which can be filled with water to adjust the buoyancy of the prototype. The overall weight of the submerged prototype (after the buoyancy cavity is filled with water) is about $2.68\,\mathrm{kg}$ with the compliant arms and about $2.84\,\mathrm{kg}$ with the addition of the compliant web. The silicone web interconnects with the arms along their side, for half of their length, starting from the arms' bases. With the arms positioned at $45°$ offset, each part of the web between two adjacent arms was designed to have the shape of an isosceles trapezoid of height $100\,\mathrm{mm}$, but with the large base being concave with a height of about $25\,\mathrm{mm}$. This configuration facilitated the extension of the silicone web when the arms are fully opened, without posing any constraints in their movement. The robotic prototype is fully untethered and energetically autonomous (powered by an on-board Li-Po battery), allowing for about 1 hour of continuous operation. An *Arduino pro mega* microcontroller platform is used to program the arm trajectories and implement various swimming gaits. Communication between the microcontroller and a local PC is achieved wirelessly through a dedicated RF link (RFM22B-S2, at $433\,\mathrm{MHz}$ ISM). Information about the position and orientation of the robotic prototype inside the water tank, where experiments are conducted ($200\,\mathrm{cm}$ x $70\,\mathrm{cm}$ x $60\,\mathrm{cm}$), is estimated by computer vision methods with a high-definition camera via a checkerboard marker of known size placed on the robot (Fig. 9a-V).

The forces generated by the arm-swimming gaits are measured with the test-rig shown in Fig. 13a via a high-precision digital force gauge (Alluris FMI-210A5). The measurement data are acquired from the force gauge via a custom interface running under LabView in the host PC.

V. EXPERIMENTAL RESULTS

In the following, we present experimental results of arm-swimming with the robotic prototype described in the previous Section. Tests involved assessing the propulsion performance under the various forward sculling gaits, for the arms alone (both for the PU and the silicone ones), as well as for the passively-compliant web.

A. Arm-swimming using only the compliant arms

The tests conducted for swimming using only the arms confirmed the generation of forward propulsion, for all of the investigated gaits $G1$, $G2$, and $G4$. The qualitative characteristics of the gaits' velocity profiles were found to be consistent with those identified in simulation. The velocities attained by the robot with the PU arms, for different A and ψ values, in gait $G1$, are shown in Fig. 10. In line with the simulation results (cf. Fig. 5), the dependence of V on the offset angle appears to be moderate. On the other hand, the experimental results suggest that the influence of the sculling amplitude is somewhat larger than predicted by our model. Such discrepancies may be attributed to the imperfect regulation of buoyancy, the limited size of the water tank (parts of the arms may protrude from the surface of the water or be in contact with the sides of the tank), or inaccuracies in vision-based estimation of the swimmer pose.

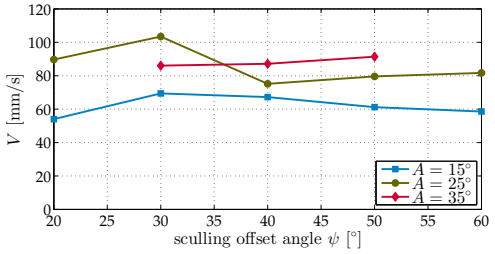

Fig. 10: Experimental results: Average velocities attained with the use of the PU arms, for gait $G1$.

The range of velocities attained with the silicone arms was about the same as for the PU arms, generally exhibiting trends comparable to the simulations.

B. Arm-swimming using the compliant arms and web

Experiments with the web-equipped variant of the prototype involved forward swimming using gait $G1$, which resulted in an overall motion of the robot (cf. Fig 11) closely resembling that of the real octopus during arm swimming (additional details are provided in Section V-D).

A summary of the velocities attained by the prototype during these experiments is provided in Fig. 12. As indicated by the maximum values of V in this plot (up to $180\,\mathrm{mm/s}$), the use of the web affords a considerable increase in the propulsive efficacy of the system, compared to swimming using only the arms. However, the results suggest that these performance gains depend upon appropriate selection of the sculling parameters, as the velocity drops off quite rapidly with ψ. We note that these findings are in close agreement with the corresponding simulation results (cf. Fig. 8).

C. Cost of Transport (CoT)

The Cost of Transport (CoT) of the system is given by the non-dimensional quantity $CoT = P_{in}/(Vmg)$, where P_{in} denotes the average electrical power consumed by the servos driving the arms during a sculling period, m is the mass of the swimming platform with the 8 arms (PU or silicone) and with or without the web, V is the average swimming velocity, and g is the acceleration of gravity.

In the experiments with the PU arms, P_{in} is approximately constant and equal to $2.8\,\mathrm{W}$, in those with the silicone arms it is approximately $2.5\,\mathrm{W}$, and in the ones with the silicone arms and web it is approximately $3.5\,\mathrm{W}$ (for the range of parameters presented above). Therefore, the variation of the CoT, for each of the above configurations, follows mostly that of the corresponding velocities. The optimal values of CoT for propulsion with the PU arms, the silicone arms, and the silicone web-arm combination, were calculated as 0.84, 0.85, and 0.62, respectively. It is worth pointing out that the web-equipped swimmer, which attains the highest propulsive velocity, is also the most energetically efficient.

D. Propulsive forces

Indicative plots for the thrust measurements obtained for arm swimming with the eight-arm robot, in gait $G1$, are shown in Figs. 13b-d. Fig. 13c corresponds to arm swimming

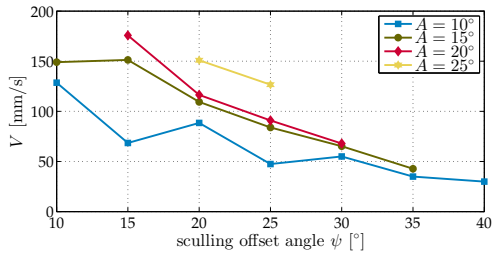

Fig. 12: Experimental results: Average velocities attained with the web-equipped variant of the prototype, for gait $G1$.

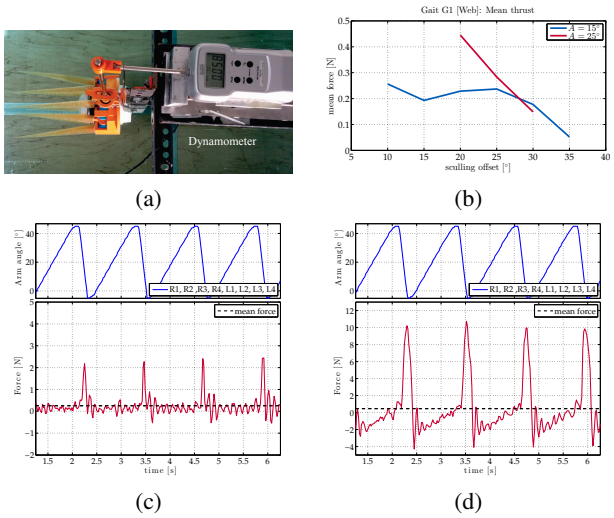

Fig. 13: (a) Set-up for force measurements. (b) Mean forces obtained for 8-arm swimming with the web in gait $G1$, as a function of the sculling offset, for two values of the sculling amplitude. (c, d) Force measurements obtained for swimming (c) with the 8 silicone arms and (d) with the arms and web, for gait $G1$ and $A = 25°$, $\psi = 20°$, $\omega = 60°$ /s, $\beta = 5$.

using only the compliant silicone arms, while Fig. 13d to arm swimming with the web. The recorded forces exhibit the same qualitative characteristics with and without the web. However, the forces, when the web is employed (mean peak force $10.45\,\mathrm{N}$), are significantly higher than those for swimming only with the arms (mean peak force $2.28\,\mathrm{N}$), for the same set of sculling parameters. Finally, the plot shown in Fig. 13b indicates that the mean generated force, for 8-arm swimming with the web generally reduces as the sculling offset is increased (while retaining the same sculling amplitude). This is in accordance with the observations made for the average swimming velocity of the system.

E. Comparisons with biology

A comparison of the 8-arm web-equipped robotic swimmer with a real octopus exhibiting arm-swimming behavior, is shown in Fig. 14. The figure captures the power stroke (of duration T_p) of one period of motion, focusing on a qualitative comparison of the velocity profile. The data for the 8-arm swimmer were obtained as indicated in Section IV, whereas those for the real octopus via a reliable 3D motion reconstruction method, described in [22], and a trinocular vision system [6], [7]. The plot indicates significant similarities in the velocity profile between the robotic swimmer and the real octopus. On closing the arms, the octopus accelerates rapidly during the early stages of the power stroke, while it slightly decelerates during the later stages. A similar pattern is exhibited by the robotic swimmer.

VI. CONCLUSIONS

The present study addresses, for the first time, the effects of arm compliance and of a compliant web on octopus-like multi-arm robotic swimming, via both computational modeling and the development of robotic prototypes. The underwater experiments performed demonstrate the efficiency of the swimmer, especially with the addition of the web, in

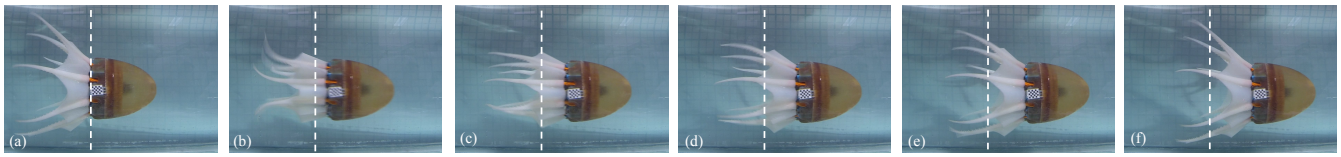

Fig. 11: Experimental results of arm-swimming with a compliant web, for gait $G1$ ($A = 15°$, $\psi = 20°$, $\omega = 50°/\,\mathrm{s}$, $\beta = 5$). Dashed line indicates the initial position of the prototype in frame (a). Frames are shown with a constant time interval of $208.5\,\mathrm{ms}$.

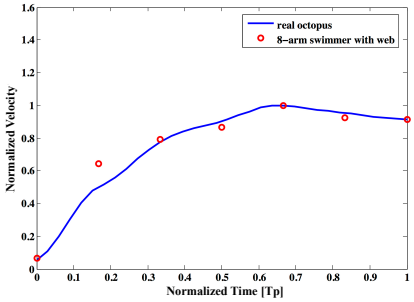

Fig. 14: Comparison between the 8-arm swimmer with the web and a real octopus in terms of normalized velocity (based on the maximum value) over normalized time duration for the power stroke ($A = 25^o$, $\psi = 40^o$, $\omega = 60^o/s$, $\beta = 5$).

terms of the attained velocities (maximum velocity: $0.18\,\mathrm{m/s}$ or 0.5 body length per second), the generated propulsive forces (maximum peak force: $10.5\,\mathrm{N}$) and the cost of transport (minimum CoT: 0.62). Moreover, they largely support the predictions of the lumped-parameter models proposed, which, although simplified, appear to capture well the behavior of the system in the operating envelope considered.

Besides straight-line swimming movements, the swimmer is able to perform turning maneuvers and crawling at the bottom of the tank. Future work will address the refinement of our models, the addition of more controlled dofs in each arm for better replicating the arm kinematics extracted from animal recordings, as well as transitions between locomotion modes and the generation of reactive behaviors.

ACKNOWLEDGMENT

The authors would like to thank B. Hochner, M. Kuba, T. Flash, F. Grasso, P.S. Krishnaprasad and J.A. Ekaterinaris for insightful discussions. Also, X. Zabulis, V. Koussanakis, P. Pandeleris and S. Stefanou, for their assistance.

REFERENCES

[1] Y. Gutfreund, T. Flash, Y. Yarom, G. Fiorito, I. Segev, and B. Hochner, "Organization of octopus arm movements: A model system for studying the control of flexible arms," *J. Neurosc.*, vol. 16, pp. 7297–7307, 1996.

[2] I. Walker, D. Dawson, T. Flash, F. Grasso, R. Hanlon, B. Hochner, W. Kier, C. Pagano, C. Rahn, and Q. Zhang, "Continuum robot arms inspired by cephalopods," in *Proc. SPIE Conf. on Unmanned Ground Vehicle Technology IV*, vol. 5804, no. 37, 2005, pp. 303–314.

[3] C. Laschi, B. Mazzolai, V. Mattoli, M. Cianchetti, and P. Dario, "Design of a biomimetic robotic octopus arm," *Bioinspir. Biomim.*, vol. 4, no. 1, pp. 015 006–1–8, 2009.

[4] R. Kang, A. Kazakidi, E. Guglielmino, D. Branson, D.P. Tsakiris, J.A. Ekaterinaris, and D. Caldwell, "Dynamic model of a hyper-redundant, octopus-like manipulator for underwater applications," in *Proc. IEEE/RSJ Int. Conf. on Int. Rob. Syst. (IROS'11)*, San Francisco, CA, September 25-30, 2011, pp. 4054–4059.

[5] C. Huffard, "Locomotion by *abdopus aculeatus* (cephalopoda: Octopodidae): Walking the line between primary and secondary defenses," *J. Exp. Biol.*, vol. 209, pp. 3697–3707, 2006.

[6] A. Kazakidi, M. Kuba, A. Botvinnik, M. Sfakiotakis, T. Gutnick, S. Hanassy, G. Levy, J. A. Ekaterinaris, T. Flash, B. Hochner, and D. P. Tsakiris, "Swimming patterns of the octopus vulgaris," in *22nd Annual Meeting NCM Society*, Venice, Italy, April 23-29, 2012.

[7] A. Kazakidi, S. Stefanou, X. Zabulis, M. Kuba, A. Botvinnik, S. Hanassy, M. Sfakiotakis, T. Gutnick, J. A. Ekaterinaris, T. Flash, B. Hochner, and D. P. Tsakiris, "Motion reconstruction of arm swimming in the octopus vulgaris," in *19th Congress of the European Society of Bioengineering (ESB)*, Patra, Greece, August 25-28 2013.

[8] M. Sfakiotakis, A. Kazakidi, N. Pateromichelakis, J.A. Ekaterinaris, and D.P. Tsakiris, "Robotic underwater propulsion inspired by the octopus multi-arm swimming," in *IEEE Int. Conf. Rob. Autom. (ICRA'12)*, St. Paul, Minnesota, USA, May 14-18, 2012, pp. 3833–3839.

[9] M. Sfakiotakis, A. Kazakidi, N. Pateromichelakis, and D.P. Tsakiris, "Octopus-inspired eight-arm robotic swimming by sculling movements," in *IEEE Int. Conf. Rob. Autom. (ICRA'13)*, Karlsruhe, Germany, May 6-10, 2013, pp. 5135—5141.

[10] M. Sfakiotakis, A. Kazakidi, and D. P. Tsakiris, "Turning maneuvers of an octopus-inspired multi-arm robotic swimmer," in *21st Med. Conf. Control Autom. (MED'13)*, Chania, Greece, June 25-28, 2013, pp. 1343–1349.

[11] V. Vavourakis, D. Bampasakis, A. Kazakidi, N. Pateromichelakis, J.A. Ekaterinaris, and D.P. Tsakiris, "Generation of primitive behaviors for non-linear hyperelastic octopus-inspired robotic arm," in *IEEE Int Conf Biomed Robotics Biomechatron*, (BioRob) Roma, Italy, 2012, pp. 725–730.

[12] V. Vavourakis, A. Kazakidi, D.P. Tsakiris, and J.A. Ekaterinaris, "A nonlinear dynamic finite element approach for simulating muscular hydrostats," *Comput. Methods Biomech. Biomed. Engin.*, vol. 17, no. 8, pp. 917–931, 2014.

[13] A. Kazakidi, V. Vavourakis, N. Pateromichelakis, J.A. Ekaterinaris, and D.P. Tsakiris, "Hydrodynamic analysis of octopus-like robotic arms," in *IEEE Int. Conf. Rob. Autom. (ICRA'12)*, St. Paul, Minnesota, USA, May 14-18, 2012, pp. 5295–5300.

[14] A. Kazakidi, V. Vavourakis, D. P. Tsakiris, and J. Ekaterinaris, "A numerical investigation of flow around octopus-like arms: near-wake vortex patterns and force development," *Comp. Meth. Biomech. Biomed. Eng.*, pp. 1–19 *in press* (doi:10.1080/10 255 842.2014.900 757), 2014.

[15] A. Kazakidi, D. P. Tsakiris, F. Sotiropoulos, and J. A. Ekaterinaris, "A computational fluid dynamic study of intense cephalopod-like motions," in *44th AIAA Fluid Dynamics Conference*, Atlanta, Georgia, 16 – 20 June 2014, pp. 1–15 (doi: 10.2514/6.2014–2504).

[16] D. Trivedi, C. D. Rahn, W. M. Kier, and I. D. Walker, "Soft robotics: Biological inspiration, state of the art, and future research," *Appl. Bionics Biomech.*, vol. 5, no. 3, pp. 99–117, September 2008.

[17] A. Villanueva, C. Smith, and S. Priya, "A biomimetic robotic jellyfish (robojelly) actuated by shape memory alloy composite actuators," *Bioinspir. Biomim.*, vol. 6, p. 036004 (16pp), 2011.

[18] A. Villanueva, K. Marut, T. Michael, and S. Priya, "Biomimetic autonomous robot inspired by the *Cyanea capillata* (Cyro)," *Bioinspir. Biomim.*, vol. 8, p. 046005 (18pp), 2013.

[19] "http://www.festo.com/net/supportportal/files/293541/."

[20] M. Sfakiotakis and D.P. Tsakiris, "SIMUUN: A simulation environment for undulatory locomotion," *Int. J. Model. Simul.*, vol. 26, no. 4, pp. 4430–4464, 2006.

[21] G. Batchelor, *An Introduction to Fluid Dynamics*. Cambridge University Press, 2000.

[22] Y. Yekutieli, R. Mitelman, B. Hochner, and T. Flash, "Analyzing octopus movements using three-dimensional reconstruction," *J. Neurophysiol.*, vol. 98, pp. 1775–1790, 2007.